Int. J. Heat Mass Transfer. Vol. 28, No. 1, pp. 183–190, 1985
Printed in Great Britain

0017-9310/85 $3.00 + 0.00
Pergamon Press Ltd.

Free convection above a near horizontal semi-infinite heated surface embedded in a saturated porous medium

D. A. S. REES and D. S. RILEY
School of Mathematics, University of Bristol

(*Received* 4 *June* 1984)

Abstract—The free convective boundary layer above a near-horizontal heated flat surface bounding a saturated porous medium is studied. Two configurations are considered: one where the component of the buoyancy force along the surface aids the flow, the other where it opposes the flow. Series solutions are developed: one valid near the leading edge, where the flow is driven along by an induced pressure gradient, and for the favourable case only, a second valid asymptotically far along the boundary, where the flow is driven along by the direct action of buoyancy forces. The description is completed by a numerical solution based on a scheme by Keller and Cebeci, which gives a step-by-step solution throughout the boundary layer. In the unfavourable case, the boundary layer separates and a region of reverse-flow develops.

1. INTRODUCTION

THE HEAT transfer and flow induced by buoyancy effects in a saturated porous medium have been studied extensively. This is quite natural because of important engineering applications such as geothermal energy resource and oil reservoir modelling and the analysis of insulating systems.

In a recent paper, Riley and Rees [1] studied steady free convection in an infinite wedge of saturated highly porous material. The region was bounded by a heated flat surface, at an angle δ to the gravity vector, and a second thermally insulated (or cold) flat surface at an angle α to the heated surface (see Fig. 1). Two distinct cases were considered in the paper: (i) the heated surface was upward-facing and horizontal ($\delta = \pi/2$) and (ii) it was upward- or downward-facing at a finite angle above the horizontal. In both cases, it was assumed that the flow was of boundary layer type, driven in (i) by an induced pressure gradient and in (ii) by the direct action of buoyancy forces. It was noted that as $\delta \to \pi/2$, a flow regime must occur where both driving mechanisms are of the same order (as $\delta \to -\pi/2$, the boundary layer assumption breaks down). This is analogous to the flow studied by Jones [2] for a Newtonian fluid. It is the purpose of this note to consider this transition problem. Thus the heated surface is taken to be upward-facing and at an angle γ to the horizontal (Fig. 1); when γ is positive the buoyancy forces aid the flow, when γ is negative they oppose it. In terms of a suitably defined Rayleigh number, consideration is given to inclinations such that $\gamma = 0(Ra^{-1/3})$ with $Ra \gg 1$. Moreover, as in [1], a generalized form of the Darcy equation relating pressure gradient to velocity is used in order to investigate inertial effects, which arise when the medium is highly porous or when the flow rates are high. In fact, only leading-order terms are considered here and the relation reduces, in the limit, to the usual Darcy form.

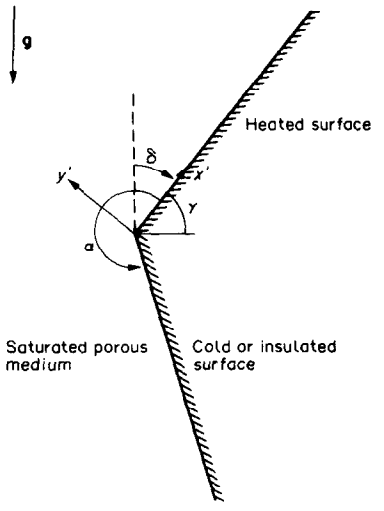

FIG. 1. Flow domain and coordinate system.

Near the leading edge of the heated surface, the fluid has absorbed so little heat that the component of the buoyancy force along the surface is weak compared with the pressure gradient induced by the hydrostatic balance normal to the surface. Further along the surface, however, the positions are reversed and the buoyancy forces dominate. When $\gamma > 0$ both mechanisms accelerate the fluid along the surface to a final state described by the free-convection solution solution for a vertical surface found by Daniels and Simpkins [3]. An interesting situation occurs when $\gamma < 0$ for, as the driving mechanisms now oppose each other, a region of reverse-flow develops. This phenomenon of boundary layer separation in a porous medium is apparently novel, as there seems to be no literature covering this aspect.

In Section 2, the boundary layer equations are derived and it is shown that, to leading order, the flow is Darcian. In Section 3, series solutions valid near the leading edge are derived for both positive and negative inclinations. A further asymptotic solution valid far

NOMENCLATURE

g	acceleration due to gravity
G	$=\left(\frac{\rho}{\mu}\right)^2 g\beta k\tilde{k}(T_w - T_0)$, dimensionless parameter
$k, \tilde{k}$	viscous and inertial impedences, respectively
L	length scale
p	total pressure, (equation 1) or dynamic pressure (equations 3 and 4)
Ra	$=\rho g\beta(T_w - T_0)kL/\mu\kappa$, Darcy–Rayleigh number
T_w, T_0	surface and ambient temperatures, respectively
(x', y')	Cartesian coordinates
(u, v)	velocity components.

Greek symbols

α	wedge angle
β	coefficient of cubical expansion
γ	angle of inclination of heated surface to the horizontal
δ	angle of inclination of heated surface to the gravity vector
ζ	$=\tilde{y}/\tilde{x}^{1/2}$, similarity variable
η	$=\tilde{y}/\tilde{x}^{2/3}$, similarity variable
θ	dimensionless temperature
κ	effective thermal diffusivity
λ	eigenconstant
μ	coefficient of viscosity
ξ	$=\tilde{x}^{1/3}$
ρ	density
τ	$=\tilde{x}^{1/2}$
ψ	stream function
Λ	$Ra^{1/3}\sin\gamma$.

along the plate is found in Section 4, for positive inclinations only. This expansion includes eigensolutions which arise from the neglect of initial conditions: the first eigensolution corresponds to a shift of the origin of the coordinate along the heated surface. Finally, in Sections 5 and 6, respectively, a brief outline of the methodology used in the numerical solution and a discussion of the results are given.

2. GOVERNING EQUATIONS

Steady, two-dimensional flow above a heated, near-horizontal, semi-infinite boundary embedded in a saturated porous medium is considered. The boundary is maintained at a uniform temperature T_w, which is above the ambient temperature T_0 of the saturated medium. In order to accommodate possible inertial effects arising from high flow rates or high porosity, we take as our constitutive relation (see [4]):

$$-\frac{k}{\mu}[\text{grad}\, p + \rho\mathbf{g}] = \left[1 + \frac{\tilde{k}}{\mu}\rho q\right]\mathbf{q}, \tag{1}$$

which reduces to Darcy's law if $\tilde{k} = 0$. Here k is the permeability of the medium and $\tilde{k}$ a material parameter, which may be thought of as a measure of its inertial impedance. $\mathbf{q}$ is velocity, ρ fluid density, μ coefficient of viscosity and p is the total pressure. A fuller discussion of this relation may be found in [1].

On assuming thermodynamic equilibrium between the saturating fluid and the solid matrix, and invoking the Boussinesq approximation, the governing equations become:

$$\frac{\partial u}{\partial x'} + \frac{\partial v}{\partial y'} = 0 \tag{2}$$

$$\left[1 + \frac{\tilde{k}}{\mu}\rho q\right]u = \frac{k}{\mu}\left[-\frac{\partial p}{\partial x'} + \beta\rho g(T - T_0)\sin\gamma\right] \tag{3}$$

$$\left[1 + \frac{\tilde{k}}{\mu}\rho q\right]v = \frac{k}{\mu}\left[-\frac{\partial p}{\partial y'} + \beta\rho g(T - T_0)\cos\gamma\right] \tag{4}$$

$$u\frac{\partial T}{\partial x'} + v\frac{\partial T}{\partial y'} = \kappa\left[\frac{\partial^2 T}{\partial x'^2} + \frac{\partial^2 T}{\partial y'^2}\right] \tag{5}$$

where $\mathbf{q} = (u, v)$, T is temperature, β the coefficient of cubical expansion of the saturating fluid, κ the effective thermal diffusivity and p now denotes dynamic pressure. Introducing dimensionless variables:

$$(x', y') = L(x, y) \qquad \theta = \frac{T - T_0}{T_w - T_0} \tag{6}$$

and dimensionless stream function ψ such that

$$\mathbf{q} = \frac{\kappa}{L}\left(\frac{\partial\psi}{\partial y}, -\frac{\partial\psi}{\partial x}\right) \tag{7}$$

we obtain, on eliminating the pressure

$$\left[1 + \frac{G}{Ra}Q\right]\nabla^2\psi + \frac{G}{QRa}[\psi_x^2\psi_{xx} + 2\psi_x\psi_y\psi_{xy} + \psi_y^2\psi_{yy}] = Ra[\theta_y\sin\gamma - \theta_x\cos\gamma] \tag{8}$$

and

$$\psi_y\theta_x - \psi_x\theta_y = \nabla^2\theta. \tag{9}$$

In the above, L denotes an arbitrary length scale, ∇^2 denotes the two-dimensional Laplacian and $Q =$

$[\psi_x^2+\psi_y^2]^{1/2}$ is the dimensionless speed. The parameter G:

$$G=\left(\frac{\rho}{\mu}\right)^2 g\beta k\tilde{k}(T_w-T_0) \tag{10}$$

is a measure of the inertial effects, whilst Ra is a Rayleigh number:

$$Ra=\frac{\rho g\beta(T_w-T_0)kL}{\mu\kappa}. \tag{11}$$

Chang and Cheng [5] showed that when $\gamma=0$ and the Rayleigh number is large boundary layer approximations to the governing equations may be obtained by introducing the scaled variables

$$\psi=Ra^{1/3}\bar{\psi},\quad y=Ra^{-1/3}\bar{y} \tag{12}$$

and ignoring terms which are $O(Ra^{-2/3})$ relative to the retained terms as $Ra\to\infty$. In the corresponding non-Darcy case, the scalings (12) again yield the boundary-layer approximation, but the relative error is $O(Ra^{-1/3})$.

The range of inclinations γ to be considered here is determined by the requirement that the buoyancy term is formally comparable with the induced pressure gradient along the heated surface. Thus on introducing (12) into (8) and (9), and taking x, θ, G and Λ as $O(1)$ as $Ra\to\infty$, where $\Lambda=Ra^{1/3}\sin\gamma$, the resulting equations are

$$\frac{\partial^2\bar{\psi}}{\partial\bar{y}^2}=\Lambda\frac{\partial\theta}{\partial\bar{y}}-\frac{\partial\theta}{\partial x} \tag{13}$$

$$\frac{\partial^2\theta}{\partial\bar{y}^2}=\frac{\partial\bar{\psi}}{\partial\bar{y}}\frac{\partial\theta}{\partial x}-\frac{\partial\bar{\psi}}{\partial x}\frac{\partial\theta}{\partial\bar{y}}. \tag{14}$$

By setting $\Lambda=0$ in (13), the system for the horizontal configuration is recovered, whilst the vertical configuration corresponds to $\Lambda\to\infty$, in which case the above scalings become inappropriate. Λ itself may be scaled out of the problem by the transformation

$$(\tilde{x},\tilde{y},\tilde{\psi})=(\Lambda_+^3x,\Lambda_+^2\bar{y},\Lambda_+\bar{\psi}), \tag{15}$$

where $\Lambda_+=\mathrm{abs}(\Lambda)$ and $\Lambda\neq0$, giving

$$\frac{\partial^2\tilde{\psi}}{\partial\tilde{y}^2}=\mathrm{sign}\,(\Lambda)\frac{\partial\theta}{\partial\tilde{y}}-\frac{\partial\theta}{\partial\tilde{x}} \tag{16}$$

$$\frac{\partial^2\theta}{\partial\tilde{y}^2}=\frac{\partial\tilde{\psi}}{\partial\tilde{y}}\frac{\partial\theta}{\partial\tilde{x}}-\frac{\partial\tilde{\psi}}{\partial\tilde{x}}\frac{\partial\theta}{\partial\tilde{y}}. \tag{17}$$

The appropriate boundary conditions are

$$\tilde{\psi}=0,\quad \theta=1\quad\text{on}\quad\tilde{y}=0\quad\text{for}\quad\tilde{x}>0$$

$$\frac{\partial\tilde{\psi}}{\partial\tilde{y}},\quad\theta\to0\quad\text{as}\quad\tilde{y}\to\infty,\quad\tilde{x}>0 \tag{18}$$

$$\text{and as}\quad\tilde{x}\to0,\ \tilde{y}>0.$$

3. SOLUTION NEAR THE LEADING EDGE

As previously noted it is anticipated that near the leading edge the structure of the boundary layer is similar to that for the horizontal configuration. This may be seen from (15), for the solution to (13) and (14) for Λ_+ small, x finite corresponds to the solution of (16) and (17) for $\tilde{x}$ small. In consequence, we use the same similarity variables as Chang and Cheng, but allow the similarity functions to have a weak dependence on $\tilde{x}$ in order to account for departures from similarity. Thus we take

$$\tilde{\psi}=\xi f(\eta,\xi),\quad\theta=g(\eta,\xi),\quad\xi=\tilde{x}^{1/3} \tag{19}$$

where the similarity variable η is given by

$$\eta=\tilde{y}/\tilde{x}^{2/3}, \tag{20}$$

and the governing system becomes

$$3\frac{\partial^2 f}{\partial\eta^2}=(2\eta\pm3\xi)\frac{\partial g}{\partial\eta}-\xi\frac{\partial g}{\partial\xi} \tag{21}$$

$$3\frac{\partial^2 g}{\partial\eta^2}+f\frac{\partial g}{\partial\eta}=\xi\left(\frac{\partial f}{\partial\eta}\frac{\partial g}{\partial\xi}-\frac{\partial g}{\partial\eta}\frac{\partial f}{\partial\xi}\right) \tag{22}$$

subject to

$$f(0,\xi)=0\quad g(0,\xi)=1$$

$$\frac{\partial f}{\partial\eta}(\eta,\xi),\quad g(\eta,\xi)\to0\quad\text{as}\quad\eta\to\infty. \tag{23}$$

In the above, the plus sign is taken for positive inclinations, and the minus sign for negative inclinations.

For small $\tilde{x}$, these equations have solutions in the form of series:

$$f=\sum_{j=0}\xi^j f_j(\eta),\quad g=\sum_{j=0}\xi^j g_j(\eta) \tag{24}$$

where the coefficient functions satisfy:

$$3f_j''=2\eta g_j'-jg_j\pm3g_{j-1}'$$

$$3g_j''=\sum_{k=0}^{j}\{k(g_kf_{j-k}'-f_kg_{j-k}')-f_kg_{j-k}'\} \tag{25}$$

with $j=0,1,2,\ldots$ and $g_{-1}\equiv0$; primes denote differentation with respect to η. The corresponding boundary conditions are

$$f_j(0)=0,\quad g_j(0)=\delta_{0j}\quad\text{and}$$

$$f_j',g_j\to0\quad\text{as}\quad\eta\to\infty \tag{26}$$

where δ_{0j} is one if $j=0$ and zero otherwise. The set of equations (25) were integrated by a Runge–Kutta–Merson procedure. The equations for f_0, g_0, which are precisely those considered in [1] and [5], were solved by a shooting technique, whilst the higher-order functions, which satisfy linear equations, were solved by the method of complementary functions. The dimensionless velocity component along the heated surface and wall heat transfer are calculated to be:

$$\left(\frac{\partial\tilde{\psi}}{\partial\tilde{y}}\right)_{\tilde{y}=0}=1.055748\xi^{-1}\pm0.651112$$

$$+0.057733\xi+0(\xi^2) \tag{27}$$

$$-\left(\frac{\partial\theta}{\partial\tilde{y}}\right)_{\tilde{y}=0} = 0.430213\xi^{-2} \pm 0.116915\xi^{-1} - 0.002274 + 0(\xi) \quad (28)$$

for small ξ; the plus and minus signs correspond to positive and negative inclinations, respectively.

4. THE ASYMPTOTIC EXPANSION FOR $\Lambda > 0$

In this case the flow structure is akin to that found by Daniels and Simpkins [3] for the vertical configuration. Guided by this, we write

$$\tilde{\psi} = \tau\hat{f}(\zeta,\tau), \quad \theta = \hat{g}(\zeta,\tau) \quad (29)$$

where

$$\zeta = \tilde{y}/\tilde{x}^{1/2}, \quad \tau = \tilde{x}^{1/2},$$

so that (16) to (18) become

$$2\frac{\partial^2\hat{f}}{\partial\zeta^2} = \left(2+\frac{\zeta}{\tau}\right)\frac{\partial\hat{g}}{\partial\zeta} - \frac{\partial\hat{g}}{\partial\tau} \quad (30)$$

$$2\frac{\partial^2\hat{g}}{\partial\zeta^2} = -\hat{f}\frac{\partial\hat{g}}{\partial\zeta} + \tau\left(\frac{\partial\hat{f}}{\partial\zeta}\frac{\partial\hat{g}}{\partial\tau} - \frac{\partial\hat{f}}{\partial\tau}\frac{\partial\hat{g}}{\partial\zeta}\right) \quad (31)$$

$$\hat{f}(0,\tau) = 0, \quad \hat{g}(0,\tau) = 1$$
$$\frac{\partial\hat{f}}{\partial\zeta}(\zeta,\tau), \quad \hat{g}(\zeta,\tau) \to 0 \quad \text{as} \quad \zeta \to \infty. \quad (32)$$

For $\tau \gg 1$, asymptotic solutions to these equations may be developed in the form:

$$\hat{f} = \sum_{j=0} \tau^{-j}\hat{f}_j(\zeta), \quad \hat{g} = \sum_{j=0} \tau^{-j}\hat{g}_j(\zeta) \quad (33)$$

with

$$2\hat{f}_j'' = 2\hat{g}_j' + \zeta\hat{g}_{j-1}' - (j-1)\hat{g}_{j-1}$$
$$2\hat{g}_j'' = -\sum_{k=0}^{j} \hat{f}_{j-k}\hat{g}_j' + \sum_{k=0}^{j-1}(k+1) \times \{\hat{f}_{k+1}\hat{g}_{j-k-1}' - \hat{g}_{k+1}\hat{f}_{j-k-1}'\} \quad (34)$$

$$\hat{f}_j(0) = 0, \quad \hat{g}_j(0) = \delta_{0j} \quad \text{and} \quad f_j', g_j \to 0 \quad \text{as} \quad \zeta \to \infty \quad (35)$$

Here $j = 0, 1, 2, \ldots, \hat{g}_{-1} \equiv 0$ and primes denote differentiation with respect to ζ. The form of the above series is correct for the analysis as far as it has been taken, but, in general, there may be logarithmic terms and also eigensolutions corresponding non-integral powers of τ.

The problem for $(\hat{f}_0, \hat{g}_0)$ has previously been solved by Singh and Cowling [6], whilst it is straightforward to show (see [3]) that $g_1 \equiv 0$. The solution for $(\hat{f}_2, \hat{g}_2)$ is given by the leading-edge shift eigensolution:

$$(\hat{f}_2, \hat{g}_2) = \frac{\lambda}{\hat{g}_0'(0)}(-\hat{f}_0 + \zeta\hat{f}_0', \zeta\hat{g}_0'), \quad (36)$$

where λ is an arbitrary constant. After solving for $\hat{f}_1$ numerically, the dimensionless velocity component along the heated surface and wall heat transfer are determined by

$$\left(\frac{\partial\tilde{\psi}}{\partial\tilde{y}}\right)_{\tilde{y}=0} = 1 + 0.808063\tau^{-1} + 0(\tau^{-3}) \quad (37)$$

$$-\left(\frac{\partial\theta}{\partial\tilde{y}}\right)_{\tilde{y}=0} = 0.443748\tau^{-1} - \lambda\tau^{-3} + 0(\tau^{-4}). \quad (38)$$

5. THE NUMERICAL SOLUTION

A complete numerical solution is effected by using a Keller box scheme [8] to integrate (21) and (22) from

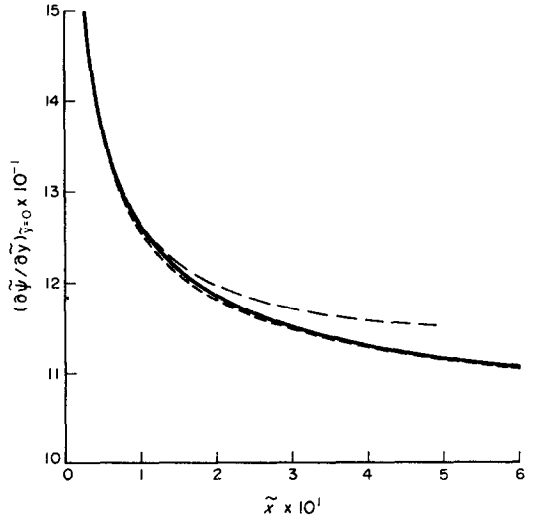

FIG. 2. Variation of slip velocity with $\tilde{x}$ when $\Lambda > 0$. (— —) 3-term expansion near $\tilde{x} = 0$. (-----) 3-term asymptotic expansion.

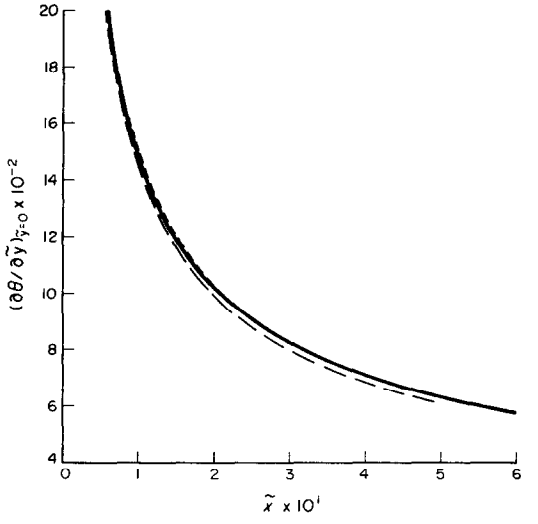

FIG. 3. Variation of surface heat transfer with $\tilde{x}$ when $\Lambda < 0$. (— —) 3-term expansion near $\tilde{x} = 0$. (----) 3-term asymptotic expansion.

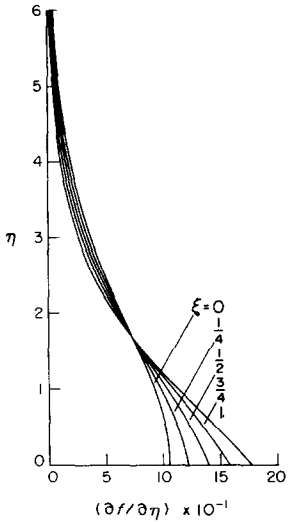

FIG. 4. Velocity profiles for $\tilde{x} \leqslant 1$ when $\Lambda > 0$.

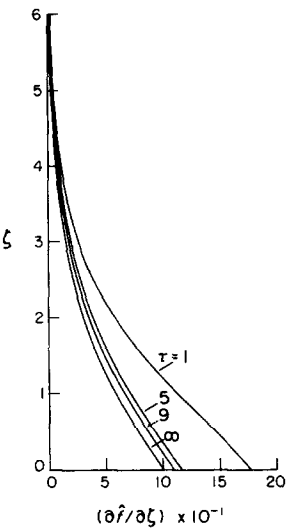

FIG. 6. Velocity profiles for $\tilde{x} \geqslant 1$ when $\Lambda > 0$.

$\xi = 0$ to $\xi = 1$, and then (30) and (31) from $\xi = \tau = 1$ onwards. The governing equations are rewritten as a system of first-order equations and then discretized on a crude non-uniform mesh. For definiteness, discussion will be in terms of the solution to (21) and (22); the solution to the other equations follow a similar pattern.

Denoting the mesh points in the (ξ, η)-plane by ξ_i and η_j, where $i = 0, 1, \ldots, M$ and $j = 0, 1, \ldots, N$, central difference approximations are made, such that those equations involving ξ explicitly are centred at $(\xi_{i-1/2}, \eta_{j-1/2})$ and the remainder at $(\xi_i, \eta_{j-1/2})$, where $\eta_{j-1/2} = \frac{1}{2}(\eta_j + \eta_{j-1})$, etc. There results a set of non-linear difference equations for the unknowns at ξ_i in terms of their values at ξ_{i-1}. These equations are conveniently and efficiently solved by using Newton iteration, taking the initial iterate to be given by the converged solution at $\xi = \xi_{i-1}$. The boundary layer equations are thus solved step-by-step.

To initiate the process the solution is required along $\xi = 0$, where the governing equations reduce to

$$\frac{\partial^2 f}{\partial \eta^2} - \frac{2}{3}\eta \frac{\partial g}{\partial \eta} = 0 \tag{21a}$$

$$\frac{\partial^2 g}{\partial \eta^2} + \frac{1}{3} f \frac{\partial g}{\partial \eta} = 0 \tag{22a}$$

subject to

$$f(0) = g(0) - 1 = 0 \quad \text{and} \quad \frac{\partial f}{\partial \eta}, \; g \to 0 \quad \text{as} \quad \eta \to \infty. \tag{23a}$$

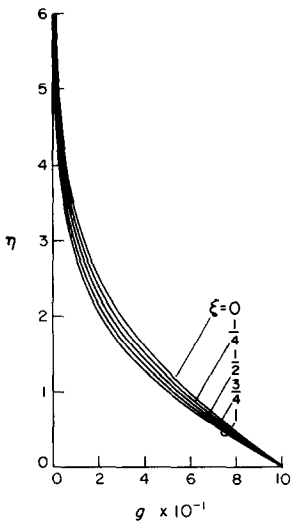

FIG. 5. Temperature profiles for $\tilde{x} \leqslant 1$ when $\Lambda > 0$.

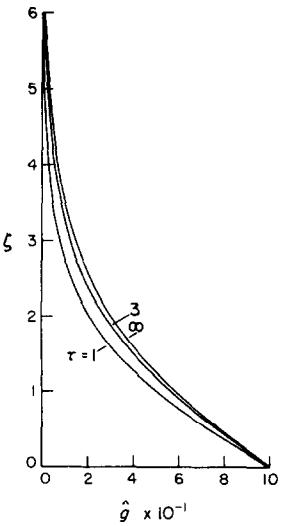

FIG. 7. Temperature profiles for $\tilde{x} \geqslant 1$ when $\Lambda > 0$.

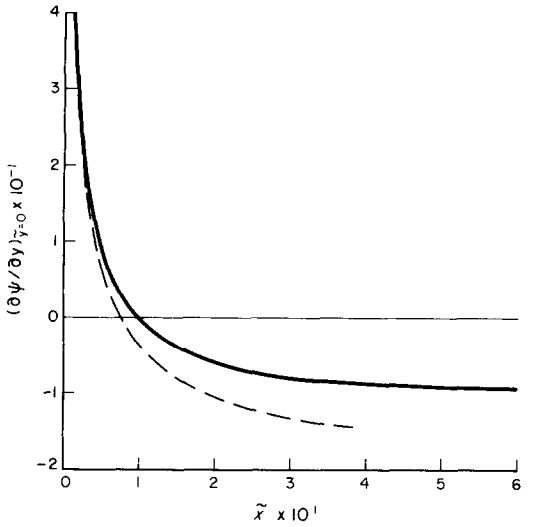

FIG. 8. Variation of slip velocity with $\tilde{x}$ when $\Lambda < 0$. (— —) 3-term expansion near $\tilde{x} = 0$.

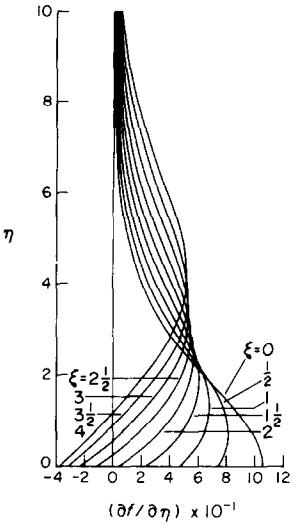

FIG. 10. Velocity profiles when $\Lambda < 0$.

As this system is precisely that given by (25) and (26) with $j = 0$, it proved convenient to employ the solution furnished by the Runge–Kutta–Merson procedure. Thus this solution is used as an initiator in a Keller box scheme for the equations along $\xi = 0$ i.e. the equations above. After obtaining a converged solution along $\xi = 0$, this solution is then employed in a Keller box scheme for equations (21) and (22) to march step-by-step along the boundary layer. In following this procedure, difficulties such as extrapolation leading to incorrect results (Wilks and Hunt [7]) were not encountered.

The basic Keller scheme possesses second-order accuracy, but, since the local truncation errors have asymptotic expansions in even powers of the mesh lengths [8], application of Richardson extrapolation may increase the accuracy by two orders. Thus, by successive applications of interval reduction and extrapolation, the truncation errors were reduced to the sixth order. Computations were performed for $0 \leqslant \tilde{x} \leqslant 64$ and $0 \leqslant \eta, \zeta \leqslant 30$, the latter range ensured that both the thermal and momentum boundary layers were contained within the integration domain, whilst the former range facilitated excellent agreement between the numerical and asymptotic results. All calculations were performed using double-precision arithmetic in order to minimize the effects of rounding errors and to take full advantage of the error reducing properties of the extrapolation procedure (the eigenconstant λ (equation 36) was thereby calculated to

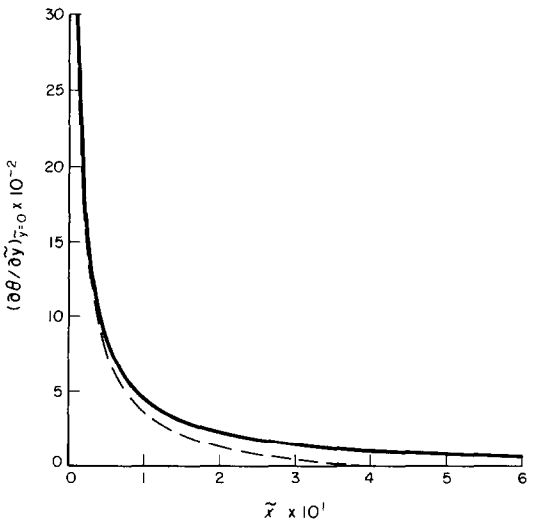

FIG. 9. Variation of surface heat transfer with $\tilde{x}$ when $\Lambda < 0$. (— —) 3-term expansion near $\tilde{x} = 0$.

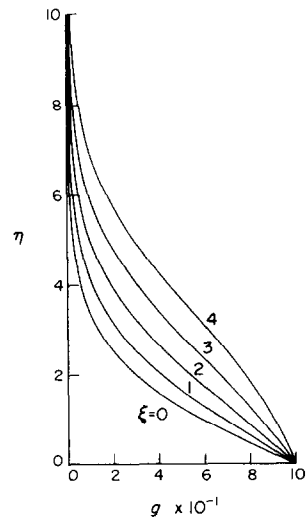

FIG. 11. Temperature profiles when $\Lambda < 0$.

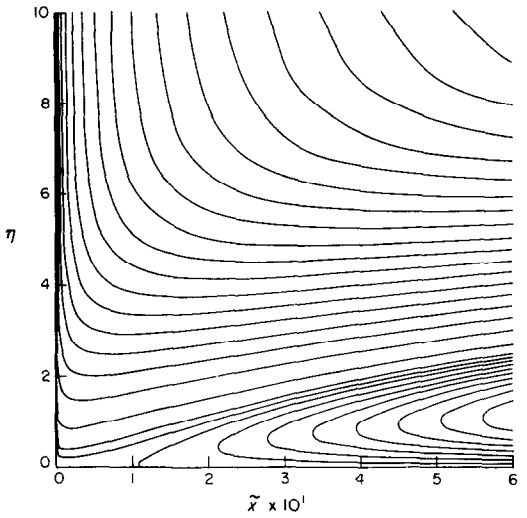

FIG. 12. Streamline plot when $\Lambda < 0$.

three significant figures). A basic net of 41 × 37 points was used, together with Richardson extrapolation based on three subnets. These subnets were obtained by subdividing each interval of the basic net into 2, 3 and 4 subintervals, respectively.

6. RESULTS AND DISCUSSION

The results of the numerical solution for $\Lambda > 0$ are presented in Figs 2–7. In Figs 2 and 3, respectively, graphs are shown of the dimensionless slip velocity $(\partial\tilde{\psi}/\partial\tilde{y})_{\tilde{y}=0}$ and wall heat transfer $-(\partial\theta/\partial\tilde{y})_{\tilde{y}=0}$. The corresponding results calculated from the series solutions (27) and (37) and (28) and (38), respectively, are superimposed on these graphs and the excellent agreement is noteworthy. By comparing (38) with the asymptotic numerical results, it is found that $\lambda \simeq -0.313$.

The developments of the velocity and thermal profiles are depicted in Figs 4 and 5 for $\tilde{x} \leqslant 1$, and in Figs 6 and 7 for $\tilde{x} \geqslant 1$. From these graphs it is seen that both the thermal and momentum boundary layers apparently decrease in thickness as $\tilde{x}$ increases. It should be noted, however, that the plots are made using the similarity variables, and in terms of physical coordinates the boundary layers actually thicken as $\tilde{x}$ increases.

For negative inclinations, $\Lambda < 0$ 'separation' occurs and a region of reverse flow develops. In Figs 8 and 9, the variation of the dimensionless slip velocity and wall heat transfer with $\tilde{x}$ are presented and compared with the series solutions (27) and (28). The slip velocity changes sign at $\tilde{x} = 9.8638$ according to the full numerical solution, compared with $\tilde{x} = 7.5664$ as given by the three-term series solution (27). Again the series solution is very good for $\tilde{x} < 2$. The developments of the velocity and temperature profiles are shown in Figs 10 and 11. In this adverse case, the boundary layer thickens substantially and the profile develops an inflexion point as the plate is traversed. Although it should not be expected that the step-by-step integration may be continued in the region of reversed flow, where the coefficient of $\partial T/\partial x'$ changes sign in (5), the numerical solution was continued as far as $\tilde{x} = 64.0$ without any obvious signs of instability. Finally in Fig. 12, a plot of the streamlines is presented which clearly shows the reverse flow region and fluid entrainment at the edge of the boundary layer.

Acknowledgement—One of us (DASR) should like to thank the SERC for the Research Studentship which enabled this research to be undertaken.

REFERENCES

1. D. S. Riley and D. A. S. Rees, Non-Darcy natural convection from arbitrarily inclined heated surfaces in saturated porous media. To appear *Quart. J. Mech. appl. Math.*
2. D. R. Jones, Free convection from a semi-infinite flat plate inclined at a small angle to the horizontal, *Quart. J. Mech. appl. Math.* **26**, 77–98 (1973).
3. P. G. Daniels and P. G. Simpkins, The flow induced by a heated vertical wall in a porous medium, *Quart. J. Mech. appl. Math.* **37**, 339–354 (1984).
4. J. Bear, *Dynamics of Fluids in Porous Media*, Elsevier, New York (1972).
5. I-Dee Chang and P. Cheng, Matched asymptotic expansions for free-convection boundary layers adjacent to flat plates in porous media, *Int. J. Heat Mass Transfer* **26**, 163–174 (1983).
6. K. R. Singh and T. G. Cowling, Thermal convection in magnetohydrodynamics, *Quart. J. Mech. appl. Math.* **16**, 1–31 (1963).
7. G. Wilks and R. Hunt, The assimilation of a strong, two-dimensional laminar jet into an aligned uniform stream, *Proc. Roy. Soc. Edin.* **90A**, 13–23 (1981).
8. H. B. Keller and T. Cebeci, Accurate numerical methods for boundary layer flows 1. Two dimensional laminar flows, *Proc. Int. Conf. Numerical Methods in Fluid Dynamics.* Lecture Notes in Physics 8, Springer, New York (1971).

CONVECTION NATURELLE AU DESSUS D'UNE SURFACE CHAUDE SEMI-INFINIE ET PRESQUE HORIZONTALE, NOYEE DANS UN MILIEU POREUX SATURE

Résumé—On étudie la couche limite de convection naturelle au dessus d'une surface plane horizontale limitant un milieu poreux saturé. Deux configurations sont considérées : l'une ou la composante de force d'Archimède le long de la surface aide l'écoulement, l'autre où elle est opposée à l'écoulement. Des solutions séries sont développées : l'une valable près du bord d'attaque où l'écoulement est favorisé par un gradient de pression induit, et dans le cas favorable seulement, une seconde valable asymptotiquement loin le long de la frontière où l'écoulement est poussé par l'action directe des forces d'Archimède. La description est complétée par une solution numérique basée sur un schéma de Keller et Cebecci, qui donne une solution pas-à-pas à travers la couche limite. Dans le cas défavorable, la couche limite se sépare et il se développe une région de courant de retour.

FREIE KONVEKTION ÜBER EINER NAHEZU HORIZONTALEN HALBUNENDLICHEN BEHEIZTEN OBERFLÄCHE, DIE SICH IN EINEM GESÄTTIGTEN PORÖSEN MEDIUM BEFINDET

Zusammenfassung—Es wird die Grenzschicht bei freier Konvektion über einer ebenen, nahezu horizontalen, beheizten Oberfläche untersucht, an die ein gesättigtes poröses Medium angrenzt. Zwei Möglichkeiten werden betrachtet: bei der einen weist die oberflächenparallele Komponente der Auftriebskraft in Strömungsrichtung, bei der anderen gegen die Strömungsrichtung. Als Lösung werden zwei Reihenentwicklungen aufgestellt: eine, die in der Nähe der Anströmkante gültig ist, wo die Strömung durch einen aufgeprägten Druckgradienten hervorgerufen wird, und—nur für den günstigen Fall—eine zweite, die in einiger Entfernung davon entlang der Begrenzung gültig ist, wo die Strömung unmittelbar durch die Auftriebskräfte hervorgerufen wird. Die Beschreibung wird vervollständigt durch eine numerische Lösung, die auf dem Verfahren von Keller und Cebeci beruht, welches eine schrittweise Lösung über die Grenzschicht liefert. Im ungünstigen Fall löst sich die Grenzschicht ab, und ein Rückströmungsgebiet bildet sich aus.

СВОБОДНАЯ КОНВЕКЦИЯ НАД ПОЧТИ ГОРИЗОНТАЛЬНОЙ ПОЛУБЕСКОНЕЧНОЙ НАГРЕВАЕМОЙ ПОВЕРХНОСТЬЮ, ПОГРУЖЕННОЙ В НАСЫЩЕННУЮ ЖИДКОСТЬЮ ПОРИСТУЮ СРЕДУ

Аннотация—Исследуется свободноконвективный пограничный слой на почти горизонтальной нагреваемой плоской поверхности, которая является границей насыщенной жидкостью пористой среды. Рассматриваются два случая: (1) составляющая подъемной силы, направленная вдоль поверхности, совпадает по направлению с течением и (2) эта составляющая подъемной силы направлена против течения. Методом разложения в ряд получены решения: одно – для области вблизи передней кромки, где поток движется под действием градиента давления, только для случая, когда подъемная сила действует по направлению течения, и второе решение, которое является асимптотически справедливым почти вдоль всей границы, где продольное движение происходит в основном под действием подъемной силы. Дано численное решение, основанное на схеме Келлера и Себеси, позволяющей получить решение в узлах сетки по всему пограничному слою. В случае, когда подъемная сила направлена против течения, пограничный слой оттесняется и развивается область возвратного течения.